



1 **Estimate of Greenland and Antarctic ice-sheet total discharge**
2 **from multiple GRACE solutions**

3 Ida Russo¹, Guillaume Ramillien², Frédéric Frappart² and Frédérique Rémy²

4

5 ¹Centro Euro-Mediterraneo per i Cambiamenti Climatici, Bologna, Italy

6 ²LEGOS, Observatoire Midi-Pyrénées, Toulouse, France

7 *Corresponding author address:* Dr. Ida Russo, Salita Moiariello 68 – 80131 Naples, Italy.

8 *Email:* ida.russo@email.it

9 **Abstract**

10 In this work a method for the estimation of 2003-2010 monthly-mean total discharge from
11 Greenland and Antarctica is presented. We show that measurements of time-variable gravity
12 from GRACE when combined with estimates of precipitation and sublimation can
13 realistically reconstruct the total discharge from the ice-sheets into the ocean. In particular, the
14 total discharge has been calculated as a 8-member ensemble-mean obtained by combining
15 multiple GRACE solutions with water fluxes from both an high resolution regional
16 atmospheric climate model (RACMO2) and a global reanalysis (ERA-Interim). The
17 gravimetric measurements of mass variations and the precipitation and sublimation
18 atmospheric fields have been combined in the ice-sheets water mass balance equation,
19 according to the main drainage basin systems. The use of the combined land-atmosphere
20 water mass balance has also been tested, which however led to a large underestimation of
21 total discharge. A comparison among the different GRACE solutions is also performed,
22 highlighting similarities and differences and analyzing the possible causes. GRACE datasets
23 show similar ice-sheet mass trends on Antarctica and over the majority of the Greenland
24 basins, while significant differences (up to a factor of 1.9) have been found in mass-loss areas
25 characterized by strongly negative water height trends. This is likely primarily caused by the



26 different pre-processing techniques applied to the raw gravimetric data.



27 **1- Introduction.**

28 Freshwater inputs to the ocean from land-ice and terrestrial water storage changes
29 represent, along with the thermal expansion of sea waters, the major cause of global sea level
30 change on short time-scales (IPCC AR5, 2014).

31 Antarctica and Greenland ice-sheets represent the vast majority of the Earth's ice.
32 Satellite-based observations and SMB (surface mass balance) model simulations show a rapid
33 acceleration of ice discharge from Greenland and Antarctica ice-sheets since 1992, by
34 contributing of about 0.6 mm/yr to the rate of global sea level rise (Shepherd et al., 2012). The
35 increasing ice mass loss from the polar ice-sheets is in particular due to an acceleration of
36 flow speed of large West Antarctica outlet glaciers system (IMBIE team, 2018) and to an
37 increase in runoff from the surface water melting in Greenland (Enderlin et al., 2014).
38 Furthermore, recent observations suggest that ice dynamics may be a key factor in the
39 response of coastal glaciers and ice-sheets melting especially in West Antarctica (Flament and
40 Rémy, 2012). In Greenland, laser altimetric observations indicate a thickening of the high
41 central ice-sheet during the 2003-2007 period, but also a significant increased loss from
42 coastal outlet glaciers, due to surface melting and accelerated flow, has occurred (Zwally et
43 al., 2011). Ice thickness surveys by NASA's Operation IceBridge suggest that, since 2009,
44 surface mass balance rather than ice dynamics has dominated Greenland contribution to sea
45 level rise (Enderlin et al., 2014). The Antarctic ice-sheet system is more complex, and
46 presents large regional differences. Ice loss in West Antarctica is mostly due to the
47 acceleration of outlet glaciers and, as a secondary effect, to enhanced melting caused by
48 increasing temperature. In contrast, surface temperatures over most of East Antarctica are
49 well below the freezing point and a small increase in air temperature cannot initiate melt
50 (Stoddart et al., 2008). The cause of acceleration of other large outlet glaciers in West



51 Antarctica is not fully understood, but may be related to sea-ice shelf instability (Holland et
52 al., 2008; Mouginit et al., 2014). In terms of equivalent sea level rise, Greenland and
53 Antarctica contributions have been estimated to be 0.17 mm/yr during the period 1992-2001
54 and 1.0 mm/yr during 2002-2011, which means that a six-fold increase in mass loss compared
55 to 1992-2001 period occurred during the recent period (IPCC AR5, 2014). Furthermore,
56 empirical methods based on the extrapolation of the ice-sheets induced sea level rise from
57 Atmosphere Ocean General Circulation Models (AOGCMs) projections, suggest that such a
58 contribution will be increasingly positive in the future (Gregory and Huybrechts, 2006).

59 Due to the increasing contribution of ice-sheets melting into the ocean and their important
60 positive contribution to sea level variations, the availability of realistic estimates of ice-sheet
61 total discharge is of major importance for the investigation and monitoring of sea level rise
62 and to understand how the Earth system is responding to anthropogenic-induced global
63 warming. If there exists no comprehensive global network for the monitoring of freshwater
64 discharge into the world oceans (Alsdorf and Lettenmaier, 2003; Brakenridge et al., 2005), the
65 situation is even worse for the Greenland and Antarctica ice sheets. Over land, river
66 discharges are unevenly distributed, discontinuous over time, and have variable accuracies. To
67 provide reliable estimates of river discharges, Fekete et al. (2000, 2002) followed a data-
68 merging approach by using observed discharge data from the Global Runoff Data Center
69 (GRDC; <http://grdc.bafg.de>) to constrain modeled estimates of runoff. Later, Dai and
70 Trenberth (2002) improved the previous work by incorporating a river-routing scheme for the
71 appropriate transport of the runoff into the ocean. Alternatively, terrestrial water storage
72 (TWS) observations from GRACE satellite gravimetry mission combined with precipitation
73 and evaporation data have been used to solve the water balance equation at basin-scale (or
74 similarly estimating precipitation and evaporation using the atmospheric water balance



75 equation) for the terrestrial freshwater discharge (Syed et al., 2007; Syed et al., 2009). In this
76 study we present a new strategy for the calculation of an ensemble of monthly ice-sheet total
77 discharge estimates, which, in the comparison with observations, has proved to be the best
78 solution to reproduce realistic estimates of Greenland and Antarctica freshwater input into the
79 ocean. According to the main drainage basin systems of the ice-sheet, we have constructed a
80 2003-2010 interannual dataset of total discharge from Greenland and Antarctica, calculated
81 by combining GRACE gravimetry observations of ice-sheets mass loss and atmospheric
82 model data of precipitation and sublimation. Differently from previous works, this is the first
83 time that such a calculation is made over the ice-sheets regions, highlighting the innovation of
84 the present study. Furthermore, multiple GRACE solutions and two different datasets of
85 atmospheric model outputs have been applied in the calculation of the total discharge
86 estimates. The importance of this study also resides in the potential application of such a
87 dataset in the frame of ocean modelling. In fact, due to the lack of time-varying runoff
88 measurements, land and ice runoff used in the current OGCMs simulations consist of
89 climatological estimates that are assumed not to vary inter-annually; the increasing freshwater
90 input from ice-sheets into the ocean is thus not considered in ocean simulations.

91 This study is structured as follows: we firstly introduce the methods (Section 2) and
92 datasets used for the total discharge calculation (Section 3); in Section 4 we show the
93 comparison among the different GRACE solutions; in Section 5 we present the results of the
94 total discharge calculation and in Section 6 the use of different precipitation datasets to
95 calculated the ice-sheet total discharge is performed and discussed; in Section 7 the main
96 conclusions are summarized followed by a discussion.

97

98



99 **2- Approaches to compute total discharge from the ice-sheets.**

100 Ice-sheet total discharge from Greenland and Antarctica were estimated by using two
101 approaches, namely through the application of the land water mass balance equation (Syed et
102 al., 2010) and the atmospheric water mass balance equation (Syed et al., 2009) over land (i.e.,
103 large river basins, drainage regions and continents). Here, we use a similar approach which is
104 described in detail below.

105

106

107 **2.1- Resolution of the surface mass balance.**

108 In the first approach, the total discharge is calculated using the ice-sheets water mass
109 balance equation:

110
$$\frac{\partial M}{\partial t} = SMB - D \quad (1)$$

111

112 where $\frac{\partial M}{\partial t}$ is the variation of mass in time over the ice-sheet; $SMB = P - E - R$ is the
113 surface mass balance, equal to the sum of solid and liquid precipitation (P), evaporation and
114 sublimation (E) and meltwater runoff (R, note that this term is negligible in Antarctica where
115 total discharge is almost totally due to ice flow; Van den Broeke et al., 2011); D is the ice
116 discharge, i.e. the iceberg calving, that is the main process through which Antarctica ice-sheet
117 is losing mass. The estimate of the total discharge (i.e. the sum of meltwater runoff R and
118 solid ice discharge D) leaving the ice-sheet is therefore equal to:

119
$$R + D = P - E - \frac{\partial M}{\partial t} \quad (2)$$

120



121 The balance was applied to the whole of Greenland and Antarctica ice-sheets according to
122 their main drainage basin systems, by computing the total volume of M, P and E within every
123 k drainage basins (Eq. (3), (4) and (5)):

$$124 \quad V_M^k(t) = \sum M(\lambda_{ij}, \theta_{ij}, t) * \cos \theta_{ij} * d\lambda_{ij} * d\theta_{ij} \quad (3)$$

$$125 \quad V_P^k(t) = \sum P(\lambda_{ij}, \theta_{ij}, t) * \cos \theta_{ij} * d\lambda_{ij} * d\theta_{ij} \quad (4)$$

$$126 \quad V_E^k(t) = \sum E(\lambda_{ij}, \theta_{ij}, t) * \cos \theta_{ij} * d\lambda_{ij} * d\theta_{ij} \quad (5)$$

127

128 where θ and λ are latitude and longitude, respectively.

129 Geographical masks of the ice-sheets drainage system regions, based on surface slopes
130 analyses, were derived from Luthcke et al. (2006) for Greenland and based on the sub-
131 division of Rignot et al. (2008) for Antarctica. Greenland was thereby divided into 6 drainage
132 basins (Figure 1) and Antarctica into 18.

133 Since GRACE data are given as monthly anomalies of mass, water storage changes are
134 considered to have occurred between the mid-point (i.e. the 15th day) of two consecutive
135 months. We have therefore computed compatible estimates of P and E by integrating daily
136 averages between the 15th day of consecutive months as follows:

$$137 \quad \int V_{R+D}^k dt = \int V_{P-E}^k dt - \left[(V_M^k)_{m+1} - (V_M^k)_m \right] \quad (6)$$

138

139 where $(V_M^k)_m$ is the total volume of M over a certain drainage basin of Greenland/Antarctica
140 expressed in equivalent water mass anomaly of the month m . This procedure was possible
141 only for daily ERA-Interim data since RACMO data were available as monthly means only.

142

143



144 **2.2- The land-atmosphere mass balance.**

145 In the second approach, the ice-sheet total discharge is computed by the use of the
146 combined land-atmosphere water mass balance equation, obtained from Eq. (1) and the
147 atmospheric moisture budget expressed as:

148
$$\frac{\partial W}{\partial t} = E - P - \nabla \cdot \vec{Q}$$
 (7)

149 where W is the total column water vapor and the last term on the right hand side is the
150 horizontal divergence of the vertically integrated vapor flux.

151 By combining Eq. (1) and (7) we therefore obtain the total discharge ($R+D$) now
152 expressed as:

153
$$R+D = -\frac{\partial M}{\partial t} - \frac{\partial W}{\partial t} - \nabla \cdot \vec{Q}$$
 (8)

154

155 On land, the method of Eq. (8) has been proved more accurate than Eq. (2) due to the large
156 uncertainty in the atmospheric models evapotranspiration that is bypassed by the use of the
157 combined land-atmosphere water mass balance equation (Syed et al. 2009). This is however
158 questionable on land-ice, where the contribution of evaporation is negligible and large
159 uncertainties on atmospheric moisture remain due to lack of a proper observational network.

160 Finally, the use of 8-member ensemble-mean total discharge has been tested. The
161 ensemble-mean solution has been calculated by averaging the eight $R+D$ fields, obtained
162 from Eq. (2), calculated by balancing, in turn, each of the four GRACE EWH dataset (JPL,
163 CSR, GFZ and GRGS) once with RACMO2 regional model data and once with ERA-Interim
164 atmospheric fields of precipitation and sublimation; these results will be discussed in detail in
165 Section 5.



166

167

168 **3- Datasets.**

169 **3.1- GRACE solutions for water mass variations.**

170 The GRACE space mission, sponsored by National Aeronautics and Space Administration
171 (NASA) and Deutsches Zentrum für Luft- und Raumfahrt (DLR), has been collecting gravity
172 variations measurements since March 2002. It provides, at regular time intervals, monthly and
173 10-day global solutions of the Earth gravity field (e.g. Wahr et al., 1998; Tapley et al., 2004;
174 Schmidt et al., 2006). These solutions are provided by different official centers as lists of
175 Stokes coefficients (i.e., spherical harmonic coefficients of the geo-potential) up to degree 50-
176 60, or equivalently at spatial resolution of 300-400 km. Changes in the gravity field are
177 largely caused by the redistribution of water mass in the hydrological cycle (Wahr et al., 1998,
178 2004). GRACE measurements have enabled for the very first time to derive satellite-based
179 global maps of terrestrial water storage variations. The Stokes coefficients are converted into
180 surface mass density and expressed in units of mm of equivalent water height (Ramillien et
181 al., 2006b). The solutions will be later called “equivalent water height differences” (EWH)
182 since they are expressed as differences between the time-variable solution and a mean static
183 gravity field.

184 In the present work we have tested the use of multiple GRACE solutions, released by
185 different research groups: Deutsches Geo Forschungs Zentrum (GFZ - Potsdam, Germany),
186 NASA Jet Propulsion Laboratory (JPL - US), Center for Space Research (CSR - US) and
187 Groupe de Recherche de Géodésie Spatiale (GRGS) at the Center National d'Etudes Spatiales
188 (CNES - Toulouse, France). These are monthly solutions at 330 km of spatial resolution (i.e.
189 up to degree 60 of the spherical harmonics). Different pre-processing methods have been used



190 to low-pass filter the high frequencies of the noise contained in the GRACE solutions.
191 Moreover, applying an Independent Component Analysis (ICA) enabled us to separate water
192 mass variations, which are meaningful geophysical signals, from the polluting noise, in
193 particular the North-South striping. This post-processing technique was only applied to the
194 CSR, GFZ and JPL data, which will be called “ICA-based” solutions in order to distinguish
195 them from the GRGS data. In this paper, the more recent releases have been used for both the
196 solutions: RL05 for ICA and RL03 for GRGS solution.

197 Once averaged over large geographical areas, the accuracy of the GRACE-estimated water
198 mass change should not exceed 1.5 cm of equivalent-water height (Wahr et al., 2004;
199 Ramillien et al, 2006a). Total errors in the Stokes coefficients are a combination of
200 instrumental and processing uncertainties, effects of the truncation of the spherical harmonic
201 spectrum (i.e., omission and leakage errors) and the lack of completeness of the dealiasing
202 models used to remove the gravitational effects of varying atmospheric and oceanic masses
203 (Velicogna and Wahr, 2013).

204 To have an idea of the mass variations of the two ice-sheets, we present the linear trends
205 (over the period 2003-2012) of EWH for the CSR solution (Figure 2). We can observe a
206 strong decrease of mass over West Antarctica (more than 10 cm/yr of equivalent water height)
207 and a slight decreasing trend over the Antarctic Peninsula. East Antarctica shows neither loss
208 nor accumulation of mass. Most of the Greenland ice-sheet is characterized by ice mass loss
209 mostly concentrated in the south-eastern part but also on the northern-west edge of the ice-
210 sheet, for the considered time frame.

211 As GRACE also detects multi-year deformation of the Earth surface such as the constant
212 Post Glacial Rebound (PGR) re-adjustment of the last deglaciation, we have to remove this
213 effect in our mass balance estimates. For this purpose, we used the global ICE-5G ice de-



214 glaciation model (Peltier, 2004; Paulson et al., 2007) to estimate the PGR trends over
215 Antarctica and Greenland. While the PGR effect is negligible for the Greenland ice-sheet, it is
216 significant on Antarctica where the PGR rate can be of the same order of magnitude as the
217 long-term ice mass change. Unfortunately, as PGR effects cannot be modelled accurately,
218 uncertainties in our PGR-related trends, and consequently on our mass balance estimates, are
219 suspected over Antarctica where the geological and long-term GPS observations that are used
220 in the PGR simulation remain rare (Peltier, 2009).

221

222

223 **3.2- Precipitation and evaporation data.**

224 For precipitation and sublimation (terms P and E in Eq. (2)), we considered two different
225 datasets: ERA-Interim atmospheric reanalyses and outputs from a regional atmospheric
226 climate model. Furthermore, we have tested the use of other datasets of precipitation in the
227 estimation of $R+D$ derived from ice-sheet water mass balance and thus compared the results;
228 these additional precipitation datasets are: CMAP, GPCP and Sheffield data.

229 ERA-Interim is third generation global atmospheric reanalysis produced by the European
230 Center for Medium-range Weather Forecasts (ECMWF). ERA-Interim covers the period from
231 1 January 1979 onwards, and continues to be extended forward in near-real time. Gridded
232 data products include a large variety of 3-hourly surface parameters, describing weather as
233 well as ocean-wave and land-surface conditions, and 6-hourly upper-air parameters covering
234 the troposphere and stratosphere. Vertical integrals of atmospheric fluxes and other derived
235 fields have also been produced (Simmons et al., 2007; Dee et al., 2011). In our work we have
236 used daily precipitation and sublimation fields at a horizontal resolution of 0.75° .
237 Furthermore, we have applied a Gaussian filter with 400 km radius, in order to be consistent



238 with the spatial resolution of GRACE data.

239 In this study we used the monthly outputs of 22-year simulations (1989-2010) performed
240 with the Regional Atmospheric Climate Model (RACMO2) at high horizontal resolution of 11
241 km over Greenland and 55 km over Antarctica (van Meijgaard et al., 2008; Ettema et al.,
242 2009). The model has been developed since 2005 at Koninklijk Nederlands Meteorologisch
243 Instituut (KNMI) and is the second version of the regional climate model RACMO. This new
244 version was built on the ECMWF physics package from cycle 23r4 embedded in the semi-
245 Lagrangian (sL) dynamics kernel of the Numerical Weather Prediction (NWP) model
246 HIRLAM5.0.6 (Undén et al., 2002). The model has been forced at the lateral boundaries and
247 at the sea surface by ERA-Interim atmospheric fluxes from ECMWF operational analyses.
248 The RACMO2 outputs consist of SMB, total precipitation and runoff fields. The sublimation
249 fields have been deduced through the simple relation $SMB = P - E - R$. Nevertheless, the
250 sublimation is not large and not very variable and the total precipitation and runoff determine
251 most of the variability.

252 Regarding the total column water vapor and the horizontal divergence of the vertically
253 integrated vapor flux, required for the coupled land-atmosphere water balance of equation (4)
254 we used only ERA-Interim data product, as these parameters are not available from RACMO.

255

256

257 **4- Comparison of GRACE solutions.**

258 In Figure 3 the comparison between the time series of equivalent water height difference
259 among all the GRACE solutions, over Greenland, East and West Antarctica, is shown. EWH
260 time series of Figure 3 show that East Antarctica is experiencing an increasing of mass, with
261 an acceleration since 2009. In contrast, West Antarctica and Greenland are losing mass since



262 2003. The former shows a mass loss acceleration developing in August 2007, while the latter
263 shows a pronounced negative trend through the whole time-span. The four GRACE datasets
264 show similar ice-sheet mass trend on Antarctica and over the whole Greenland ice-sheet. To
265 deepen our analysis, we have compared EWH time-series for the different Greenland drainage
266 basins (Figure 4), evidencing the south-east Greenland coast (*basin 4*) as the area of highest
267 mass loss of the ice-sheet, while the total discharge flux reaches its minimum values in
268 correspondence of the north-eastern edge (*basin 2*). Even if in agreement in terms of
269 maximum and minimum areas of mass change, the two groups of GRACE solutions, GRGS
270 and ICA-based solutions, show significant differences in terms of trend magnitude. The major
271 difference has been found at northern-west Greenland (*basin 1*, Figure 5 top panel), where the
272 GRGS solution present a trend almost twice higher than the ICA one, which means a
273 considerable impact in terms of equivalent sea level contribution from Greenland ice-sheet.
274 Significant differences are also evident at the eastern coast, where the EWH trend of the two
275 groups of solutions differ by a factor of 1.5 (*basin 3*) and 1.1 (*basin 2*). The difference is even
276 more amplified in the southern-east part (*basin 4*), i.e. the area of highest ice mass loss. Over
277 this particular drainage basin, the GRGS EWH time series exhibit an ice mass loss rates 1.6
278 times higher than JPL: -15.48 cm/yr with respect to -9.51 cm/yr (Figure 5, bottom panel).

279 Several causes can give rise to the marked differences in equivalent water height trends of
280 the two groups of solutions. A considerable part is attributable to the different pre- and post-
281 processing techniques applied to the two different GRACE datasets. In fact, distinct pre-
282 processing methods have been used to filter out the high frequencies from the noisy GRACE
283 solutions, in order to extract realistic hydrological signals on the continents. In particular,
284 stabilization method have been applied to Level-1 of GRGS solutions and a Gaussian filter
285 have been applied to Level-2 of CSR, GFZ, JPL solutions. The reader is referred to Wahr et



286 al. (1998) for further details on GRACE data processing. A secondary effect of Gaussian filter
287 method is to cut off the high frequencies from the EWH signal, which are then redistributed
288 and spread over the surrounding areas. In fact, if the trend computation is not limited to the
289 Greenland ice-sheet land but extended over a bigger area which also includes the surrounding
290 ocean, few degrees off Greenland coasts, we can see a better match between GRGS and ICA
291 datasets trend (Figure 6). In this case, in fact, the high frequencies, cut off by Gaussian filter
292 method and redistributed in the surrounding areas, are now included in the ICA solutions
293 trend, which now differ from GRGS by a factor of 1.4 and 1.2 for *basin 1* and *basin 4*,
294 respectively. An additional effect that further influences *basin 1* is the positive EWH trend
295 over Canada and the Canadian Arctic Archipelago, which is distinctively visible before the
296 PGR correction (see Figure 2). This effect is probably spread over the close North-West
297 Greenland with the consequence of further decreasing the negative ICA solution trend with
298 respect to the GRGS one. Another possible source of difference is the application of the ICA
299 method, employed to further filter the CSR, GFZ and JPL solutions, which has not been
300 applied to the GRGS solution. In particular, this post-processing technique has been used with
301 the aim to reduce the presence of north-south striping due to orbit resonance that limits the
302 geophysical interpretation of the signal (Frappart et al., 2010, 2011). In order to test this
303 hypothesis a comparison among EWH time-series before and after the application of the ICA
304 method has been performed (not shown). Results suggest that the application of the ICA
305 method is not responsible for the differences in EWH trends of the two groups, conversely
306 after the application of this post-processing technique, EWH time-series of the ICA-based
307 solution result to be closer to the GRGS solution tendency (not shown). Moreover, other
308 possible causes can be attributed to differences in the static gravity field removed to the time-
309 varying solution and to differences in the oceanic/atmospheric models used to dealias the



310 GRACE solutions in order to remove the atmospheric pressure influence on satellite orbits
311 and on the ocean state.

312

313

314 **5- Total discharge results.**

315 In order to validate the total discharge estimates from Greenland and Antarctica and hence
316 to assess our method as a proper strategy for the realistic reconstruction of $R+D$, we have
317 compared the results obtained from Eq. (2) and (8) with measurements of ice discharge,
318 obtained by combining maps of surface velocities along ice-sheet coasts from InSAR data and
319 ice thickness from Digital Elevation Model (DEM, Rignot et al., 2011). The comparison is
320 made by subtracting the meltwater runoff (R) from the total discharge $R+D$ in order to have
321 consistent data with InSAR observations. Note that in the case of Antarctica a direct
322 comparison is allowed, since runoff from the surface water melting is a negligible process at
323 those latitudes and mass loss happens thus almost exclusively through solid ice discharge
324 (Van den Broeke et al., 2011).

325 Results are displayed in Figure 7. Here we present the ice-discharge estimates obtained by
326 using CSR GRACE data balanced once with RACMO (green line) and once with ERA-
327 Interim (cyan line) precipitation and sublimation fields. Both estimates have been calculated
328 by means of the ice-sheets water mass balance equation (2). In the comparison (Figure 7), we
329 found that the use of precipitation and sublimation fields from RACMO regional model
330 (green line) slightly overestimates observation values (magenta line) while the use of ERA-
331 Interim (cyan line) slightly underestimates them. On the other hand, the ice discharge
332 obtained by using the combined land-atmosphere water mass balance equation (8) (blue line)
333 strongly underestimates InSAR data. In light of these results, we have decided to combine the



334 two atmospheric datasets in an ensemble-mean, by also including all the GRACE solutions.
335 The 8-member ensemble-mean solution (red line) turns out to be the curve that better fits with
336 ice discharge observations; in fact, the ensemble-mean closely follows InSAR curve, except
337 for some seasonal peaks not represented by observations. At this regard, we want to underline
338 that InSAR data are available as yearly means only and this is also the reason why they cannot
339 be used for $R+D$ estimation.

340 As a further verification of the reliability of our method, in Figure 8 we have verified the
341 correct representation of the climatological seasonal cycles of Greenland and Antarctica
342 ensemble-mean total discharge. In Antarctica (bottom panel, red line) the total discharge
343 shows two minimum in November and January, in accordance with the seasonal minimum of
344 precipitation (see Figure 9 bottom panel). Precipitation over Antarctica is more abundant from
345 March to October, which is particularly evident in the RACMO2 dataset (Figure 9 bottom
346 panel, green line). In accordance, Antarctica $R+D$ starts to increase in April reaching its
347 maximum values in June after the precipitation peak. Our results are in accordance with the
348 work of Ligtenberg et al. (2012) which using a combination of a firn densification model and
349 a regional atmospheric climate model have shown that high temperatures and low
350 accumulation cause Antarctica ice-sheet surface to low in austral summer, while in autumn,
351 winter and spring the surface steadily rises, mainly due to higher accumulation rates. It is also
352 in good accordance with seasonal change of Antarctica ice-sheet height derived from
353 altimetry (Rémy et al., 2014).

354 Also over Greenland the seasonal cycle is correctly reproduced by the ensemble-mean
355 total discharge (Figure 8 top panel, red line); the summer peak is in accordance with both
356 realistic freshwater fluxes averaged over the 1991-2000 period (Marsh et al., 2010), even if
357 shifted from June to July, and different SMB models inter-comparison (Vernon et al., 2013).



358 With this further analysis we have demonstrated that our estimated $R+D$ is representative of
359 the interannual variability of the freshwater flux from land to ocean.

360

361

362 **6- Total discharge derived from ice-sheets water mass balance with different**
363 **precipitation datasets.**

364 In this study we have chosen to perform the calculation of the ice-sheet total discharge by
365 using two datasets of precipitation: ERA-Interim and RACMO2. This choice has been made
366 in order to exploit the accurateness that a third generation reanalysis, as ERA-Interim, and
367 that the high spatial resolution of a regional atmospheric model, as RACMO2, has in itself.
368 Nevertheless, several accurate precipitation products are available. We have, hence, tested the
369 use of other datasets of precipitation in the estimation of $R+D$ derived from ice-sheet water
370 mass balance and thus compared the results. In this way, we are able to assess the robustness
371 of our method, once verified the similarity among all the resulting precipitation-derived total
372 discharge.

373 The precipitation datasets involved in the comparison are CMAP, GPCP and Sheffield
374 data. The CPC Merged Analysis of Precipitation (CMAP) is a technique which produces
375 pentad and monthly analyses of global precipitation in which observations from rain gauges
376 are merged with precipitation estimates from several satellite-based algorithms (infrared and
377 microwave). The analyses are on a $2.5^\circ \times 2.5^\circ$ degree latitude/longitude grid and extend back
378 to 1979 (Xie and Arkin, 1997).

379 The Global Precipitation Climatology Project (GPCP) was established by the World
380 Climate Research Program to quantify the distribution of precipitation around the globe over
381 many years. The precipitation product is obtained by optimally merging estimates computed



382 from microwave, infrared, and sounder data observed by the international constellation of
383 precipitation-related satellites, and precipitation gauge analyses. The product is available
384 since 1979 with horizontal resolution of $2.5^\circ \times 2.5^\circ$ (Adler et al., 2003).

385 The Sheffield dataset of precipitation (Sheffield et al., 2006) is a global, 60-yr (1948-
386 2008), 3-hourly, 1.0° dataset of land surface hydrology fields. The dataset is constructed by
387 combining a suite of global observation-based datasets (GPCP, TRMM, GSWP-2) with the
388 National Centers for Environmental Prediction–National Center for Atmospheric Research
389 (NCEP–NCAR) reanalysis.

390 In Figure 8, we compare mean seasonal ice-sheet total discharge derived with the mass
391 balance equation (Eq. 2) by using different precipitation datasets: ERA-Interim (cyan line),
392 RACMO (green line), CMAP (black line), GPCP (orange line) and Sheffield (magenta line).
393 The comparison among the precipitation products is also shown (Figure 9). We can see that
394 the various estimated $R+D$ are of the same order of magnitude on both Greenland (top) and
395 Antarctica (bottom), with RACMO and Sheffield presenting the highest values of
396 precipitation (Figure 9) and hence of total discharge values (Figure 8). Also in terms of
397 seasonal cycle, all the precipitation-derived $R+D$ show a strongly similar interannual
398 variability, presenting the same summer peaks of discharge in June and July. The similar
399 behavior detected, confirms the robustness of our method and the reliability of the
400 precipitation data, ERA-Interim and RACMO2, used in our study. It is however worthy to
401 underline that caution has to be taken when precipitation reanalyses data are used for a study
402 of Antarctica mass balance (Bromwich et al., 2011). In fact, data assimilation is still
403 challenging in this region as reanalyses rely heavily upon a small number of ground-based
404 and upper-air observations in Antarctica, especially in the interior of the ice-sheet. Moreover,
405 the wind-blown snow (or wind-driven ablation), which, on short spatial scale, greatly affects



406 the surface mass balance over Antarctica due to the presence of katabatic winds (Rémy and
407 Frezzotti, 2006), is an important process that is not taken into account in ERA-Interim
408 reanalysis.

409

410

411 **7- Conclusions.**

412 In this study, we have proposed a strategy useful for creating an ice-sheet total discharge
413 dataset by combining multiple GRACE gravimetric data of ice mass variation on land-ice
414 with atmospheric model data of precipitation and sublimation. For the atmospheric fields, we
415 have tested the use of data from both an high resolution regional model, RACMO2, and ERA-
416 Interim reanalysis. We have demonstrated the ability of our methodology to correctly
417 reproduce realistic estimates of ice-sheet total discharge for the 2003-2010 period. In
418 particular, in the comparison with InSAR satellite observations of ice discharge, it turned out
419 that the best fit with observations is achieved with an ensemble-mean of multiple GRACE
420 solutions (JPL, CSR, GFZ and GRGS data) in combination with the two atmospheric model
421 datasets. Total discharge has been computed with the ice-sheets water mass balance equation,
422 which was applied to the main drainage basins of Greenland and Antarctica, and this is the
423 first time that such a balance is applied on land-ice. We have also tested the use of the
424 combined land-atmosphere water mass balance equation, which, however, led to a large
425 underestimation of the total discharge and has not been considered further.

426 The two groups of GRACE solutions (GRGS and ICA-based solutions) show important
427 differences in the ice mass loss 2003-2012 estimates for the southeast Greenland coast and for
428 the northwestern edge of the ice-sheet, both characterized by a strong negative signal of water
429 height trend. Namely, the GRGS solutions exhibits a faster mass loss rate with respect to the



430 ICA-based, reaching a factor of 1.9 between the GRGS (-6.01 cm/yr) and the JPL (-3.22
431 cm/yr) solution over *basin 1*. The difference in the equivalent water height trends can be
432 mainly attributed to differences in the pre- processing techniques applied to the GRACE
433 solutions used to filter out the high frequencies from the noisy raw data.

434 The importance of this study also resides in the possible applications into which such an
435 interannual ice-sheet total discharge dataset can be involved, as the exploitation in global,
436 regional and coastal ocean modeling. It can be prescribed, in fact, as forcing input in ocean
437 circulation models, in order to study the response of sea level, ocean mass properties and
438 thermohaline circulation to a realistic freshwater coastal discharge. Ocean models, in fact, are
439 a powerful tool for the study of sea level change and for the investigation of the impact that
440 ice-sheet total discharge has, and could have in the future, on the ocean state and in particular
441 on sea level rise. Nevertheless, most of the current OGCMs do not take into account this
442 important source of freshwater input; in fact, due to the lack of time-varying freshwater flux
443 measurements, land runoff and ice discharge used in the current OGCMs simulations only
444 includes climatological estimates that are assumed not to vary inter-annually; therefore ocean
445 simulations cannot take into account increasing ice-sheets contribution and its variability,
446 ignoring, in this way, one of the main cause of global sea level rise.



447 **References.**

448 Adler, R.F., Huffman, G.J., Chang, A., Ferraro, R., Xie, P., Janowiak, J., Rudolf, B.,
449 Schneider, U., Curtis, S., Bolvin, D., Gruber, A., Susskind, J., and Arkin, P.: The Version 2
450 Global Precipitation Climatology Project (GPCP) Monthly Precipitation Analysis (1979-
451 Present). *J. Hydrometeor.*, 4,1147-1167, 2003.

452

453 Alsdorf, D.E., and Lettenmaier, D.P.: Tracking fresh water from space. *Science*, 301, 1491-
454 1494, 2003.

455

456 Brakenridge, G.R., Nghiem, S.V., Anderson, E., and Chien S.: Space-based measurement of
457 river runoff. *Eos, Trans. Amer. Geophys. Union*, 86, 185-188, 2005.

458

459 Bromwich, D., Nicolas, J., and Monaghan, A.: An assessment of precipitation changes over
460 Antarctica and the Southern Ocean since 1989 in contemporary global reanalyses. *Journal of*
461 *Climate*, 24, 4189-4209, 2011.

462

463 Dai, A., and Trenberth, K.E.: Estimates of freshwater discharge from continents: latitudinal
464 and seasonal variations. *Journal of hydrometeorology*, 3, 660-687, 2002.

465

466 Dee, D. P., Uppala, S. M., Simmons, A. J., Berrisford, P., Poli, P. et al.: The ERA-Interim
467 reanalysis: configuration and performance of the data assimilation system. *Quarterly Journal*
468 *of the Royal Meteorological Society*, Volume 137, pages 553-597, 2011.

469

470 Enderlin, E.M., Howat, I.M., Jeong, S., Noh, M.J., van Angelen, J.H., and van den Broeke,



471 M.R.: An improved mass budget for the Greenland ice sheet. *GRL* (41), 866-872, DOI:
472 10.1002/2013GL059010, 2014.

473

474 Ettema, J., van den Broeke, M.R., van Meijgaard, E., van de Berg, W.J., Bamber, J.L., Box,
475 J.E., and Bales, R.C.: Higher surface mass balance of the Greenland ice sheet revealed by
476 high-resolution climate modeling. *Geophys. Res. Lett.*, Vol. 36, L12501,
477 doi:10.1029/2009GL038110, 2009.

478

479 Fekete, B.M., Vörösmarty, C.J., and Grabs, W.: Global composite runoff fields based on
480 observed data and simulated water balance. Global Runoff Data Centre Tech. Rep. 22,
481 Koblenz, Germany, 108 pp, 2000.

482

483 Fekete, B.M., Vörösmarty, C.J., and Grabs, W.: High-resolution fields of global runoff
484 combining observed river discharge and simulated water balances. *Global Biogeochem.*
485 *Cycles*, 16, 1042, doi:10.1029/1999GB001254, 2002.

486

487 Flament, T., and Rémy, F.: Dynamic thinning of Antarctic glaciers from along-track repeat
488 radar altimetry. *Journal of Glaciology* 58(211): 830–840, 2012.

489

490 Frappart, F., and Ramillien, G.: Contribution of GRACE Satellite Gravimetry in Global and
491 Regional Hydrology, and in Ice Sheets Mass Balance. In the book “Water Resources
492 Management and Modeling”, edited by Purna Nayak, ISBN 978-953-51-0246-5, InTech,
493 March 3, 2012.

494



- 495 Frappart, F., Ramillien, G., Maisongrande, P., and Bonnet, M.-P.: Denoising satellite gravity
496 signals by Independent Component Analysis. *IEEE Geosci. Remote Sens. Lett.* 7 421–5, 2010.
497
- 498 Frappart, F., Ramillien, G., Leblanc, M., Tweed, S.O., Bonnet, M.-P., and Maisongrande, P.:
499 An independent component analysis approach for filtering continental hydrology in the
500 GRACE gravity data. *Remote Sens. Environ.* 115 187–204., 2011.
501
- 502 Gregory, J.M., and Huybrechts, P.: Ice-sheet contributions to future sea-level change. *Philos.*
503 *Trans. R. Soc. London Ser. A*, 364, 1709–1731, 2006.
504
- 505 Holland, D., Thomas, R.H., De Young, B., Ribergaard, M.H., and Lyberth, B.: Acceleration
506 of Jakobshavn Isbraetrigged by warm subsurface ocean waters. *Nat. Geosc.*, 2008.
507
- 508 IMBIE team: Mass balance of the Antarctic Ice Sheet from 1992 to 2017. *Nature* 558, 219-
509 222, 2018.
510
- 511 IPCC: Climate Change 2013: The Physical Science Basis. Contribution of Working Group I
512 to the Fifth Assessment Report of the Intergovernmental Panel on Climate Change [Church,
513 J.A., Clark, P.U., Cazenave, a., Gregory, J.M., Jevrejeva, S., Levermann, A., Merrifield, M.A.,
514 Milne, G.A., Nerem, R.S., Nunn, P.D., Payne, A.J., Pfeffer, W.T., Stammer, D., Unnikrishnan,
515 A.S., (eds.)]. Cambridge University Press, Cambridge, United Kingdom and New York, NY,
516 USA, 2014.
517
- 518 Ligtenberg, S. R. M., Horwath, M., Van den Broeke, M. R., and Legrésy, B.: Quantifying



519 the seasonal breathing of the Antarctic ice sheet, *Geophys. Res. Lett.*, 39, L23501,
520 doi:10.1029/2012GL053628, 2012.

521

522 Luthcke, S.B., Zwally, H.J., Abdalati, W., Rowlands, D.D., Ray, R.D., et al.: Recent
523 Greenland ice mass loss by drainage system from satellite gravimetry observations.
524 *Scienceexpress* 314:1286-89, doi:10.1126/science.1130776, 2006.

525

526 Marsh, R., Desbruyères, D., Bamber, J. L., De Cuevas, B. A., Coward, A. C., and Aksenov,
527 Y.: Short-term impacts of enhanced Greenland freshwater fluxes in an eddy-permitting ocean
528 model, *Ocean Sci.*, 6, 749-760, 2010.

529

530 Mougnot, J., Rignot, E., and Scheuchl, B.: Sustained increase in ice discharge from the
531 Amundsen Sea Embayment, West Antarctica, from 1973 to 2014. *GRL* (41), 1576–1584,
532 DOI:10.1002/2013GL059069, 2013.

533

534 Paulson, A., Zhong, S., and Wahr, J.: Inference of mantle viscosity from GRACE and
535 relative sea level data. *Geophys. J. Int.* 171, 497–508. doi: 10.1111/j.1365-
536 246X.2007.03556.x, 2007.

537

538 Peltier, W. R.: Global glacial isostasy and the surface of the Ice-Age Earth: The ICE-5G
539 (VM2) model and GRACE. *Annu. Rev. Earth Planet. Sci.*, 32, 111– 149, 2004.

540

541 Ramillien, G., Frappart, F., Güntner, A., Ngo-Duc, T., Cazenave, A., and Laval, K.: Time
542 variations of the regional evapotranspiration rate from Gravity Recovery and Climate



543 Experiment (GRACE) satellite gravimetry. *Water Resour. Res.*, 42, W10403,
544 doi:10.1029/2005WR004331, 2006a.

545

546 Ramillien, G., Lombard, A., Cazenave, A., Ivins, E., Llubes, M., et al.: Interannual
547 variations of ice sheets mass balance from GRACE and sea level. *Glob. Planet. Change*
548 53:198-208, 2006b.

549

550 Rémy, F., Flament, T., Michel, A., and Verron, J.: Ice sheet survey over Antarctica with
551 satellite altimetry: ERS1/2, Envisat, Saral/AltiKa, the key importance of continuous
552 observations along the same repeat orbit. *Int. J. Remote Sens*, 35, 5497–5512, 2014.

553

554 Rémy, F., and Frezzotti, M.: Antarctica ice sheet mass balance. *C. R. Geosci.*, 338, 1084-
555 1097, 2006.

556

557 Rignot, E., Bamber, J.L., Van den Broeke, M.R., Davis, C., Li, Y., et al.: Recent Antarctic
558 ice mass loss from radar interferometry and regional climate modelling. *Nat. Geosci.* 1:106-
559 10, 2008.

560

561 Rignot, E., Velicogna, I., van den Broeke, M.R., Monaghan, A., and Lenaerts, J.:
562 Acceleration of the contribution of the Greenland and Antarctic ice sheets to sea level rise.
563 *Geophys. Res. Lett.* 38:L05503. doi:10.1029/2011GL046583, 2011.

564

565 Schmidt, R., Flechtner, F., Reigber, Ch., Schwintzer, P., Günter, A., Doll, P., Ramillien, G.,
566 Cazenave, A., Petrovic, S., Jochman, H., and Wunsch, J.: GRACE observations of changes in



567 continental water storage. *Glob. Planet. Change* 50/1–2, 112–126.

568 doi:10.1016/j.gloplacha.2004.11.018, 2006.

569

570 Sheffield, J., Goteti, G., and Wood, E.F.: Development of a 50-yr high-resolution global
571 dataset of meteorological forcings for land surface modeling. *J. Clim.* 19:3088–3111, 2006.

572

573 Shepherd, A., Ivins, E.R., Geruo, A., and Barletta, V.R., et al.: A reconciled estimate of ice-
574 sheet mass balance. *Science* 338(6111): 1183–1189, 2012.

575

576 Simmons, A., Uppala, S., Dee, D., and Kobayashi, S.: ERA-Interim: New ECMWF
577 reanalysis products from 1989 onwards. In Newsletter 110. ECMWF, 2007.

578

579 Stoddart, D.M., et al.: Australia's Antarctic science program. *Department of the*
580 *Environment, Water, Heritage and the Arts, Australian Antarctic Division*, 2008.

581

582 Syed, T.H., Zlotnicki, V., and Rodell, M.: Contemporary estimates of Arctic freshwater
583 discharge from GRACE and reanalyses. *Geophys. Res. Lett.*, 34, L19404,

584 doi:10.1029/2007GL031254, 2007.

585

586 Syed, T.H., Famiglietti, J.S., and Chambers, D.P.: GRACE-based estimates of terrestrial
587 freshwater discharge from basin to continental scales. *J Hydrometeorol* 10:22–40, 2009.

588

589 Syed, T. H., Famiglietti, J.S., Chambers, D., Willis, J., Hilburn, K.: Satellite-Based Global
590 Ocean Mass Balance Estimates of Interannual Variability and Emerging Trends in Continental



591 Freshwater Discharge, Proc. Nat. Acad. Sci., 107 (42) 17916-17921; published ahead of print
592 October 4, 2010, doi:10.1073/pnas.1003292107, 2010.

593

594 Tapley, B.D., Bettadpur, S., Watkins, M., and Reigber, C.: The gravity recovery and climate
595 experiment: mission overview and Early results. *Geophys. Res. Lett.* 31, L09607.
596 doi:10.1029/2004GL019920, 2004.

597

598 Undén, P., Rontu, L., Järvinen, H., Lynch, P., Calvo, J., Cats, G., Cuxart, J., Eerola, K.,
599 Fortelius, C., Garcia-Moya, J.A., Jones, C., Lenderink, G., McDonald, A., McGrath, R.,
600 Navascues, B., Nielsen, N.W., Odegaard, V., Rodrigues, E., Rummukainen, M., Rõõm, R.,
601 Shattler, K., Sass, B.H., Savijärvi, H., Schreur, B.W., Sigg, R., The, H., and Tijm, A.:
602 HIRLAM-5 Scientific Documentation, HIRLAM-5 Project, c/o Per Undén SMHI, S-601 76
603 Norrköping, SWEDEN, 144 p, 2002.

604

605 van den Broeke, M.R., Bamber, J., Lenaerts, J., and Rignot, E.: Ice sheets and sea level:
606 thinking outside the box. *Surv. Geophys.* 32 495–505, 2011.

607

608 van Meijgaard, E., van Ulft, L.H., van de Berg, W.J., Bosveld, F.C., van den Hurk, B.J.J.M.,
609 Lenderink, G., Siebesma, A.P.: The KNMI regional atmospheric climate model RACMO
610 version 2.1. Technical report ; TR – 302, 2008.

611

612 Velicogna, I., and Wahr., J.: Time-variable gravity observations of ice sheet mass balance:
613 Precision and limitations of the GRACE satellite data. *Geophysical Research Letters*,
614 40(12):3055–3063, 2013. ISSN 1944-8007. doi: 10.1002/grl.50527, 2013.

615

616 Vernon, C. L., Bamber, J. L., Box, J. E., van den Broeke, M. R., Fettweis, X., Hanna, E., and
617 Huybrechts, P.: Surface mass balance model intercomparison for the Greenland ice sheet, The



- 618 Cryosphere Discuss., 6, 3999–4036, doi:10.5194/tcd-6-3999, 2012.
619
- 620 Wahr, J., Molenaar, M., and Bryan, F.: Time-variability of the Earth's gravity field:
621 Hydrological and oceanic effects and their possible detection using GRACE. *J. Geophys.*
622 *Res.*, 103, 32,20530,229, 1998.
623
- 624 Wahr, J., Swenson, S., Zlotnicki, V., and Velicogna, I.: Time-variable gravity from GRACE:
625 First results. *Geophys. Res. Lett.*, 31, L11501, doi:10.1029/2004GL019779, 2004.
626
- 627 Xie, P., and Arkin, P.A.: Global precipitation: A 17-year monthly analysis based on gauge
628 observations, satellite estimates, and numerical model outputs. *Bull. Amer. Meteor. Soc.*, 78,
629 2539-2558, 1997.
630
- 631 Zwally, H.J., Li, J., Brenner, A.C., Beckley, M., Cornejo, H.G., Dimarzio, J., Giovinetto,
632 M.B., Neumann, T.A., Robbins, J., Saba, J.L., Yi, D., and Wang, W.: Greenland ice sheet
633 mass balance: distribution of increased mass loss with climate warming: 2003-07 versus
634 1992-2002. *J. Glaciol.*, 57, 1–15, 2011.



635 **List of figure captions.**

636

637 **Figure 1**– Greenland drainage system regions based on surface slopes analyses proposed by
638 Luthcke et al. (2006).

639 **Figure 2** – Equivalent water height trend over the 2003-2012 period calculated from CSR
640 GRACE solution.

641 **Figure 3**– Time series of equivalent water height over Greenland (top), East and West
642 Antarctica (middle and bottom, respectively) from the all GRACE solutions. The time series
643 have been computed with respect to 2003-2011 average.

644 **Figure 4**– Time series of equivalent water height over the 6 drainage basins of Greenland ice-
645 sheet from JPL (top) and GRGS (bottom) solutions. JPL solution has to be intended as
646 representative of the whole ICA-based solutions.

647 **Figure 5**– Time series of equivalent water height from all the GRACE solutions, over the
648 northern-west (basin 1, top) and the southern-east (basin 4, bottom) drainage basin of
649 Greenland ice-sheet (see Figure 1 for the location of the basin).

650 **Figure 6**– Time series of equivalent water height from all the GRACE solutions, over the
651 northern-west (basin 1, top) and the southern-east (basin 4, bottom) Greenland drainage basin
652 and the surrounding ocean nearby the coasts.

653 **Figure 7**– Comparison of Greenland (top panel) and Antarctica (bottom panel) ice discharge
654 estimated from the different methods of total discharge calculation with InSAR observations
655 (magenta line).

656 **Figure 8**– Monthly climatology (2003-2010) of Greenland (top) and Antarctica (bottom)
657 ensemble-mean total discharge (red lines) and total discharge derived from ice-sheet water



658 mass balance by using different datasets of precipitation.

659 **Figure 9**– Comparison among the different precipitation datasets (2003-2010 climatologies)

660 over Greenland (top) and Antarctica (bottom).

661

662

663

664

665

666

667

668

669

670

671

672

673

674

675

676

677



678
679
680
681
682
683
684
685
686
687
688
689
690
691
692
693
694
695
696

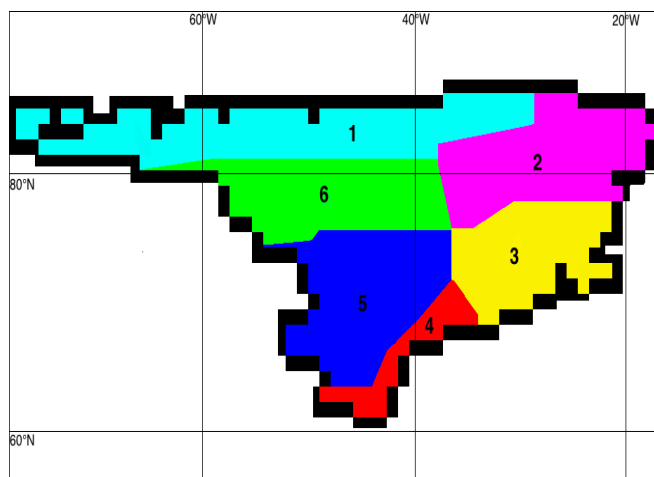


Figure 1– Greenland drainage system regions based on surface slopes analyses proposed by Luthcke et al. (2006).

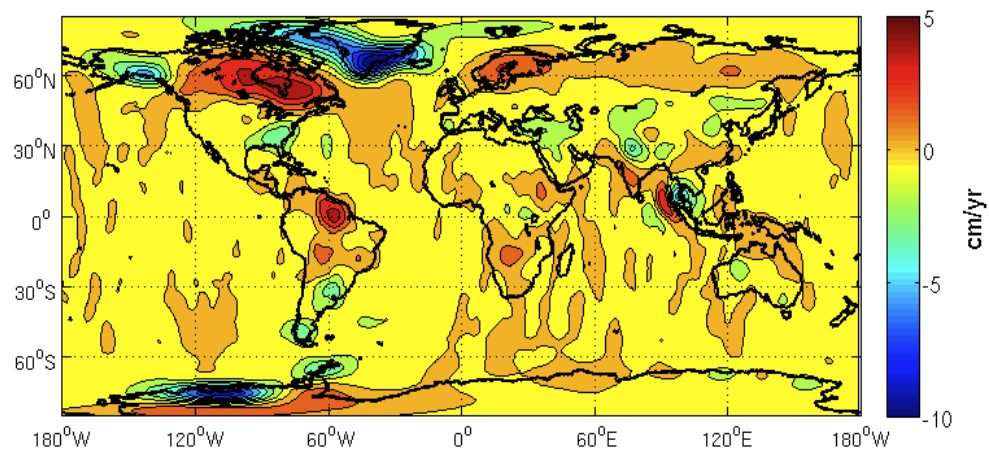
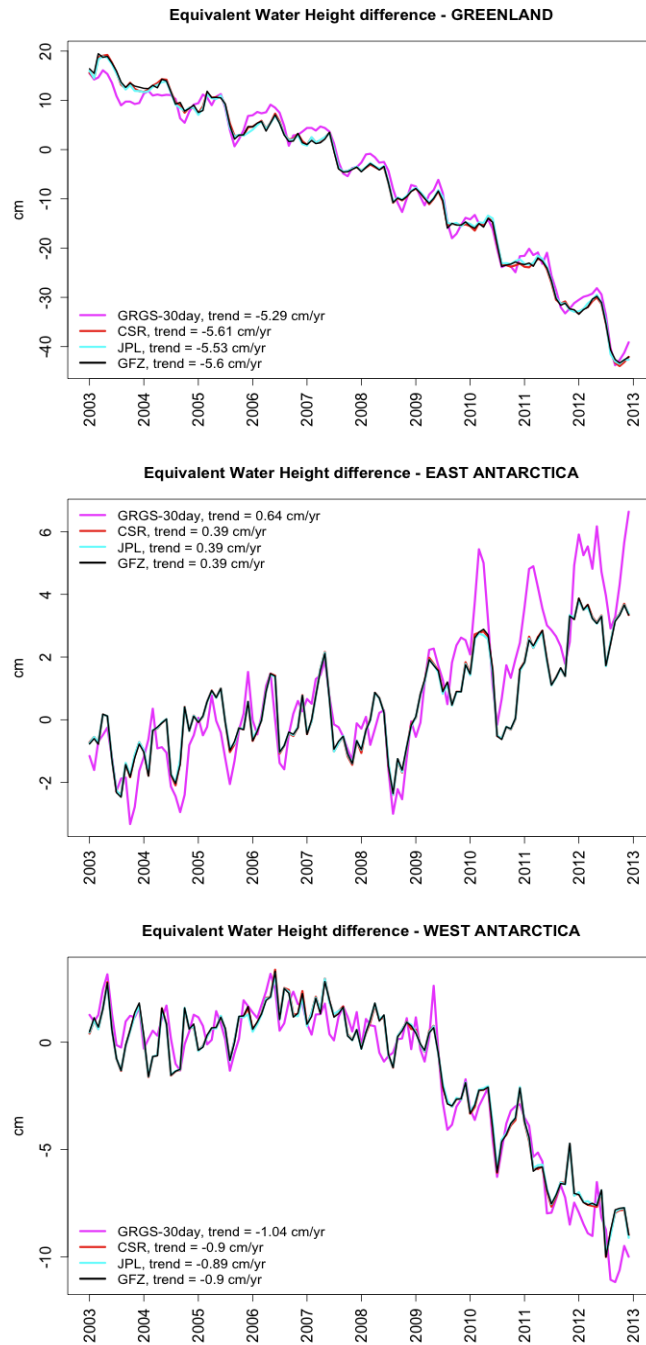


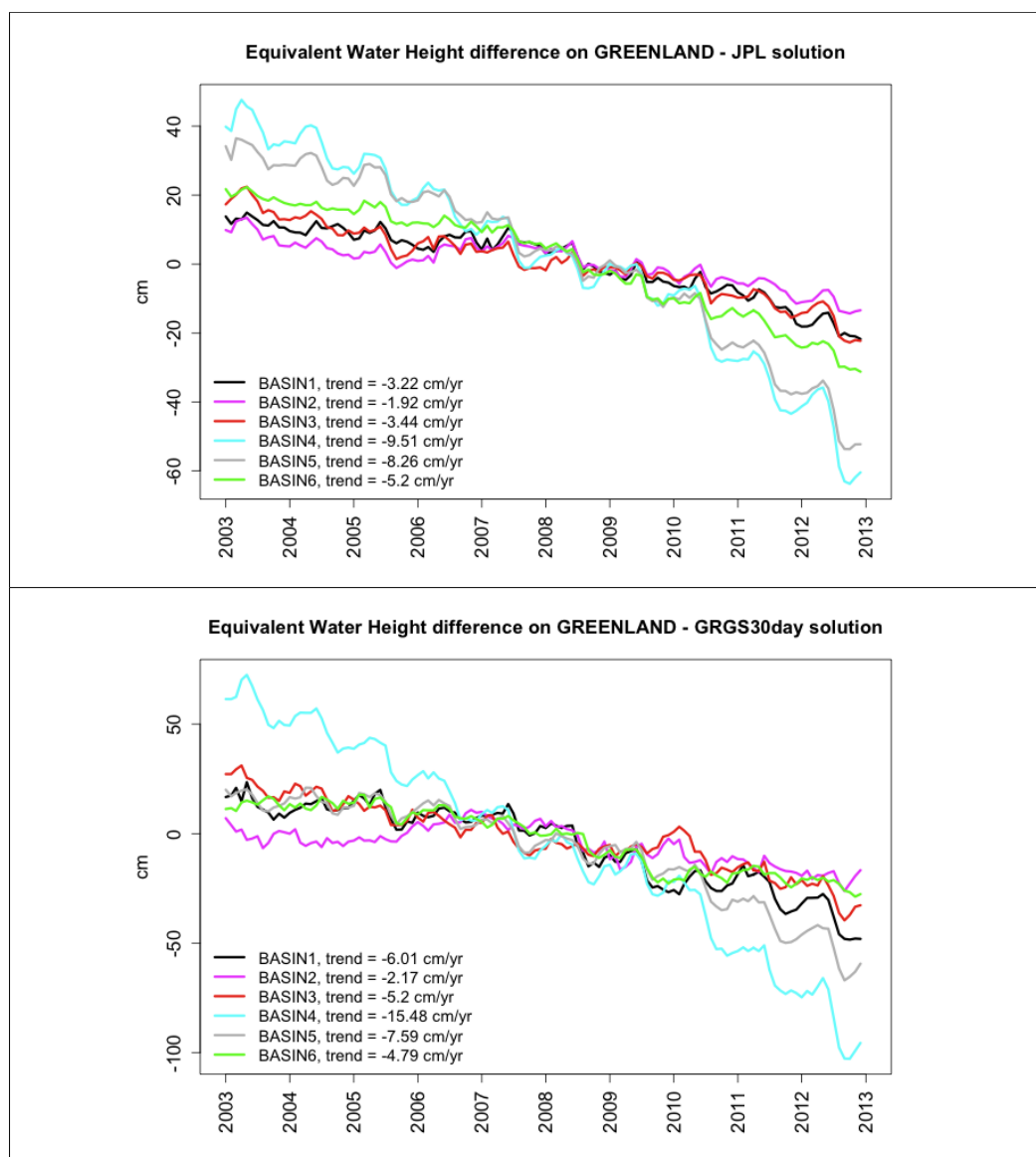
Figure 2 – Equivalent water height trend over the 2003-2012 period calculated from CSR GRACE solution.



700 **Figure 3**– Time series of equivalent water height over Greenland (top), East and West
701 Antarctica (middle and bottom, respectively) from all GRACE solutions. The time series have



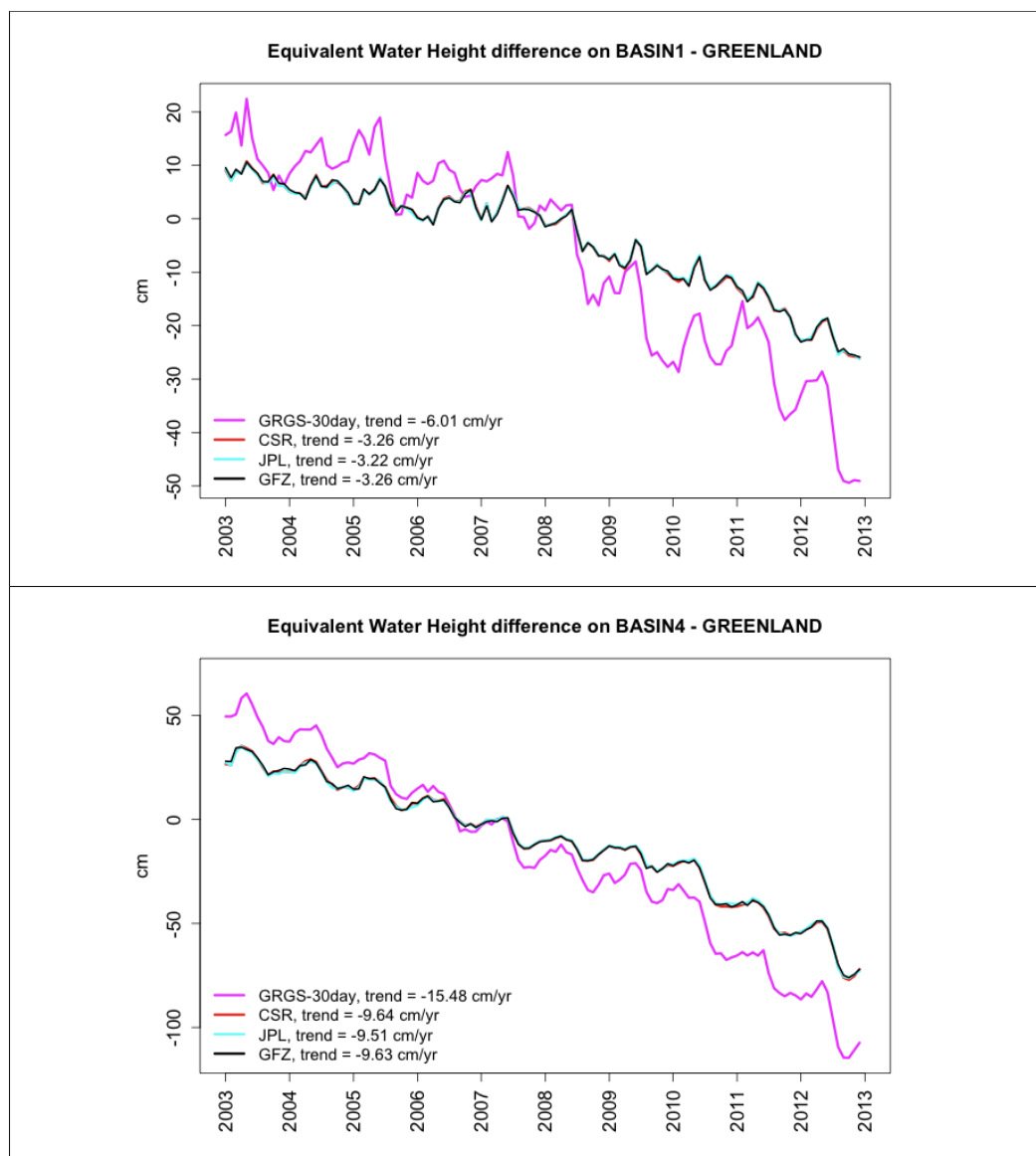
702 been computed with respect to 2003-2011 average.
703
704
705



706
707 **Figure 4**– Time series of equivalent water height over the 6 drainage basins of Greenland ice-
708 sheet from JPL (top) and GRGS (bottom) solutions. JPL solution has to be intended as
709 representative of the whole ICA-based solutions.



710



711

712 **Figure 5**– Time series of equivalent water height from all the GRACE solutions, over the
713 northern-west (basin 1, top) and the southern-east (basin 4, bottom) drainage basin of
714 Greenland ice-sheet (see Figure 1 for the location of the basin).

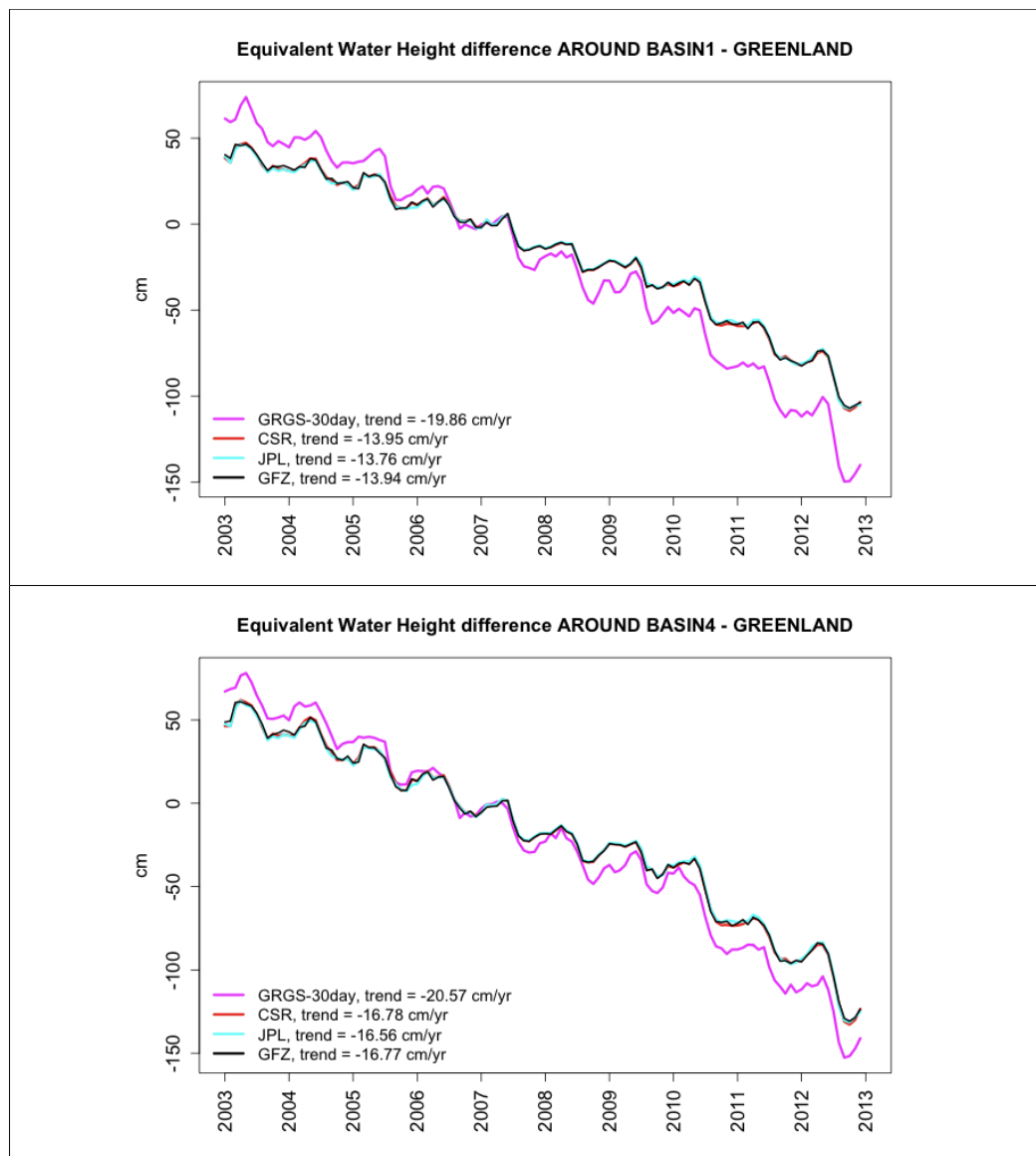
715

716

717



718



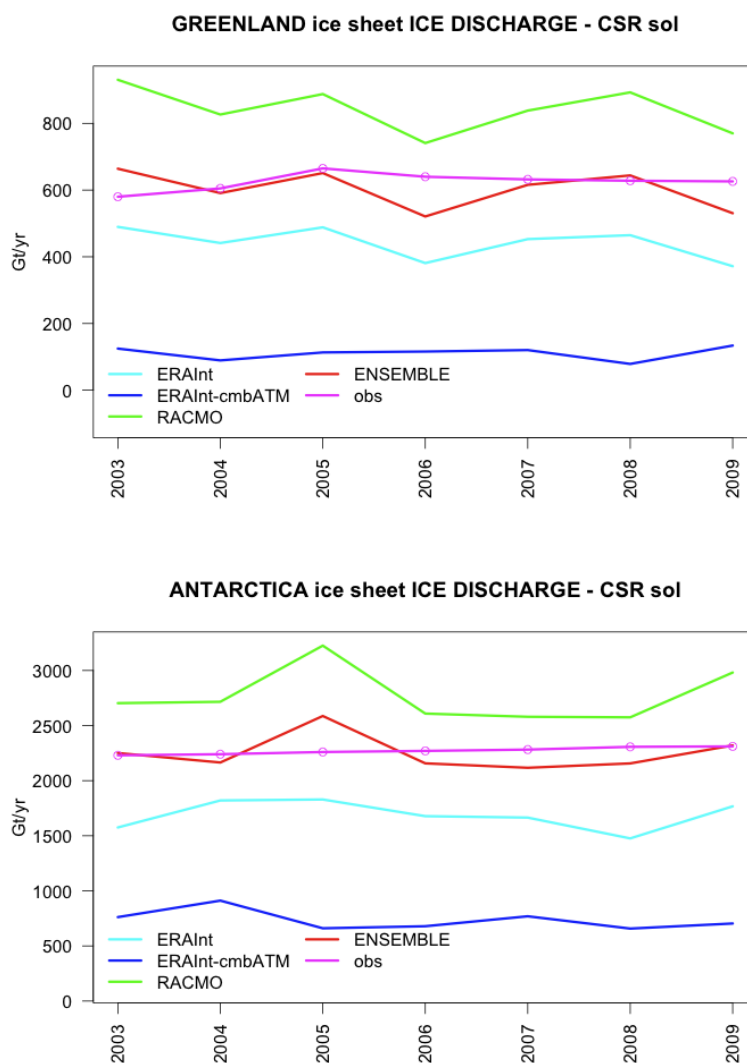
719

720 **Figure 6**– Time series of equivalent water height from all the GRACE solutions, over the
721 northern-west (basin 1, top) and the southern-east (basin 4, bottom) Greenland drainage basin
722 and the surrounding ocean nearby the coast.

723

724

725



726

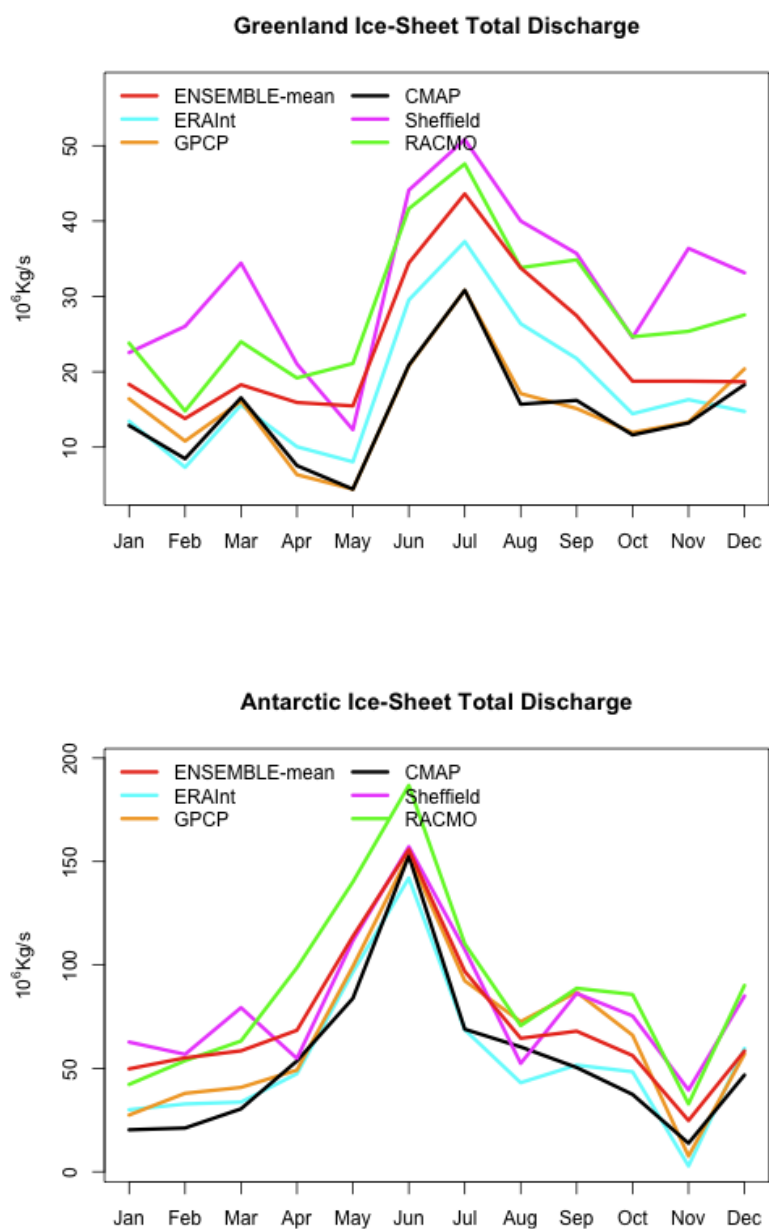
727 **Figure 7**– Comparison of Greenland (top panel) and Antarctica (bottom panel) ice discharge
728 estimated from the different methods of total discharge calculation with InSAR observations
729 (magenta line).

730

731

732

733

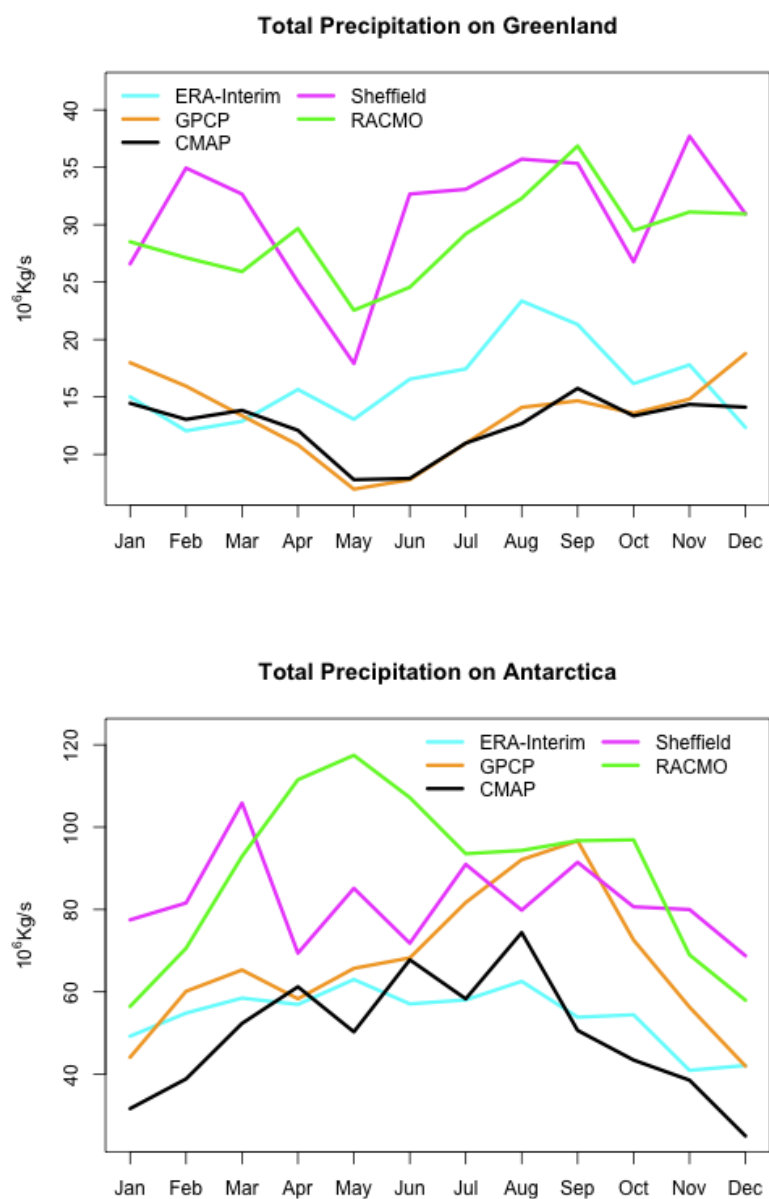


734

735 **Figure 8**– Monthly climatology (2003-2010) of Greenland (top) and Antarctica (bottom)
736 ensemble-mean total discharge (red lines) and total discharge derived from ice-sheet water
737 mass balance by using different datasets of precipitation.



738



739

740 **Figure 9**– Comparison of different precipitation datasets (2003-2010 climatologies) over
741 Greenland (top) and Antarctica (bottom).